Published in final edited form as:
Immunity. 2011 February 25; 34(2): 163–174. doi:10.1016/j.immuni.2011.02.003.

COUPLING OF V(D)J RECOMBINATION TO THE CELL CYCLE SUPPRESSES GENOMIC INSTABILITY AND LYMPHOID TUMORIGENESIS

Li Zhang[†], **Taylor L. Reynolds**, and **Xiaochuan Shan**[††,*]
Department of Molecular Biology and Genetics and Institute for Cell Engineering, The Johns Hopkins University School of Medicine, Baltimore, MD 21205, USA

Summary

V(D)J gene segment recombination is linked to the cell cycle by the periodic phosphorylation and destruction of the RAG-2 protein at the G1-to-S cell cycle transition. To examine the function of this coupling, we constructed mice in which the phosphorylation site at threonine 490 of RAG-2 was mutated to alanine. The RAG-2 T490A mutation uncoupled DNA cleavage from cell cycle and promoted aberrant recombination. Similar aberrant recombination products were observed in mice deficient in the Skp2 ubiquitin ligase subunit, which is required for periodic destruction of RAG-2. On a p53-deficient background the RAG-2 T490A mutation induced lymphoid malignancies characterized by clonal chromosomal translocations involving antigen receptor genes. Taken together these observations provide a direct link between the periodic destruction of RAG-2 and lymphoid tumorigenesis. We infer that cell cycle control of the V(D)J recombinase limits the potential genomic damage that could otherwise result from RAG-mediated DNA cleavage.

Introduction

The genes that encode antigen receptors are assembled from discrete DNA segments that are brought together during lymphocyte development by variable-diversity-joining (V(D)J) recombination (Gellert, 2002). The recombination activating gene (RAG) proteins RAG-1 and RAG-2 initiate rearrangement by cleaving participating gene segments at recombination signal sequences (RSSs). DNA cleavage produces signal ends, which terminate in flush, double-stranded breaks, and coding ends, which terminate in hairpin structures (Gellert, 2002). Recombination is completed by the RAG proteins and components of the machinery for DNA double-strand break repair (DSBR) (Fugmann et al., 2000; Gellert, 2002).

There are two general mechanisms for DSBR in eukaryotic cells: non-homologous end joining (NHEJ) and homologous recombination (HR). NHEJ, which is essential for V(D)J recombination, is carried out by a suite of proteins that includes Ku70, Ku80, artemis, DNA-PKcs, XRCC4, DNA ligase IV and XLF, also known as Cernunnos (Ahnesorg et al., 2006;

[*]Corresponding author: telephone (410) 955-4735, sdesider@jhmi.edu.
[†]Current address: Division of Pediatric Oncology, The Johns Hopkins University School of Medicine, Baltimore, MD 21231
[††]Current address: Abramson Family Cancer Research Institute, University of Pennsylvania School of Medicine, Philadelphia, PA 19104

Buck et al., 2006; Lieber et al., 2003). The importance of NHEJ in maintaining genomic stability is demonstrated by the frequent lymphoid tumors and associated chromosomal translocations observed in mice doubly deficient in NHEJ and DNA damage-induced apoptosis. Mice lacking XRCC4 and the pro-apoptotic protein p53 (Gao et al., 2000) or Ku80 (Difilippantonio et al., 2000) succumb to pro-B lymphomas carrying translocations involving *Igh* and *Myc*, consistent with a role for NHEJ in protection against oncogenic consequences of RAG-mediated DNA cleavage (Difilippantonio et al., 2000; Gao et al., 2000; Zhu et al., 2002).

In mammalian cells NHEJ predominates during the G1 and early S cell cycle phases, whereas HR and NHEJ are both employed in late S and G2 (Fukushima et al., 2001; Takata et al., 1998). The RAG proteins preferentially direct DNA ends into the NHEJ pathway, and some RAG mutations that impair joining favor repair by HR or an alternative form of NHEJ (Corneo et al., 2007; Lee et al., 2004). Initiation of V(D)J recombination is also sequestered temporally from HR by the periodic destruction of RAG-2. RAG-2 accumulates in the G0 and G1 cell cycle phases and is rapidly degraded at the G1-to-S transition (Li et al., 1996; Lin and Desiderio, 1993; Lin and Desiderio, 1994). Consequently, accumulation of recombination intermediates (Desiderio et al., 1996; Schlissel et al., 1993) and RAG-signal end complexes (Jiang et al., 2004) is restricted to G0 and G1. Destruction of RAG-2 is triggered upon phosphorylation of threonine 490 by cyclin A-Cdk2 (Jiang et al., 2005; Lee and Desiderio, 1999; Li et al., 1996), which creates a binding site for the Skp2-SCF ubiquitin ligase, a regulator of cell cycle progression (Jiang et al., 2005). Upon its polyubiquitination by Skp2-SCF, RAG-2 is degraded by the proteasome (Jiang et al., 2005).

The restriction of RAG activity to G0 and G1 limits RSS cleavage to times at which double-strand DNA repair proceeds predominantly by NHEJ. To understand the physiologic relevance of this restriction, we generated mice in which the Cdk2 phosphorylation site at threonine 490 of RAG-2 was mutated to alanine. Our observations indicate that restriction of RAG activity to the G0-G1 cell cycle phases protects against potential genomic instability arising from V(D)J recombination. Just as the RAG complex physically sequesters DNA ends from homologous recombination, so the periodic destruction of RAG-2 may sequester DNA ends temporally from alternative and potentially harmful modes of repair.

Results

A RAG-2 T490A mutation uncouples accumulation of RAG-2 and RSS breaks from the cell cycle

A mutation specifying RAG-2(T490A) was introduced into ES cells by homologous recombination, using a targeting construct bearing a neomycin resistance marker (*neo*) flanked by *lox*P sites. As a control, the wild-type *Rag2* locus was tagged with a floxed *neo* marker. The *Rag2*(T490A) allele was marked with a *Pst*I restriction site and could thus be distinguished from wild-type (Fig. 1A). ES cells were used to obtain chimeric mice capable of transmitting the modified alleles in the germline and floxed sequences were deleted by mating with *cre* transgenic females. In this way we obtained mice bearing targeted, excised wild-type (WT*)* and *Rag2*(T490A) alleles (Fig. 1B). In all experiments reported here, results were similar for wild-type (WT) mice and mice bearing the WT* allele.

Accumulation of RAG-2 was uncoupled from the cell cycle in RAG-2(T490A) mutant mice. Thymocytes were fractionated according to cell cycle phase and assessed for DNA content and RAG-2 protein. In WT*/WT* mice, as expected, RAG-2 accumulated preferentially in thymocytes with 2C DNA content (Fig. 1C). In contrast, accumulation of RAG-2(T490A) persisted throughout the cell cycle in thymocytes from homozygous mutant (T490A/T490A) mice (Fig. 1C).

Recombination signal end intermediates normally accumulate preferentially in the G0 and G1 cell cycle phases. We examined the cell cycle distribution of signal ends in pooled thymocytes from eight WT*/WT* and eight T490A/T490A mice. Recombination signal ends were assayed at three sites within the T cell receptor (TCR) β locus: the 5′ flank of Jβ2.5, the 5′flank of Dβ2 and the 3′ flank of Dβ2. In WT*/WT* mice signal ends were detected highly preferentially in G0-G1 cells (Fig. 1D), as expected. In T490A/T490A mice, however, signal ends were readily detected in the G0-G1 and S-G2-M thymocyte populations (Fig. 1D). Signal ends at the 3′ flank of Dβ2 were detected in S-G2-M phase thymocytes from mutant mice at at least half the level observed in G0-G1 phase cells (Supplemental Fig. S1). Signal ends at Vβ14, which undergoes inversional rearrangement, must be repaired to maintain chromosomal integrity; these ends were also observed to accumulate in S-G2-M phase thymocytes from mutant mice (Supplemental Fig. S1). We conclude that accumulation of RAG-2 and accumulation of recombination intermediates are uncoupled from the cell cycle in RAG-2(T490A) mutant mice.

Increased frequency of aberrant V(D)J recombination in mice expressing RAG-2(T490A)

Lymphocyte development was grossly normal in T490A/T490A mice (Fig. 2A, B). The mutant mice did, however, show decreased thymic cellularity (Fig. 2C) and an increase in the frequency of apoptotic cells in the $CD4^{-}CD8^{-}$ compartment, where TCRβ, γ and δ gene rearrangement occurs (Fig. 2D and Supplemental Fig. S2). Notably, apoptosis was similarly increased in heterozygous and homozygous mice, consistent with dominance of the T490A allele. These observations suggested that DNA ends produced by unscheduled cleavage might undergo alternative fates that invoke cell loss. We therefore sought evidence for abnormal recombination in mice expressing RAG-2(T490A).

Signal joints (SJs) generated by V(D)J recombination are more sensitive indicators of aberrant recombination than coding joints because their junctional sequences are relatively simple. We examined SJs produced by inversional recombination between the TCR gene segments Vβ14 and Dβ1 or Vδ5 and Dδ2, as these products are retained in the genome. SJs were amplified from thymocyte DNA and cloned; precise SJs were identified by *Apa*L1 digestion. The nucleotide sequences of imprecise, *Apa*L1-resistant fragments were determined. Imprecise SJs infrequently occur at TCR loci in wild-type mice, generally as a result of N region addition (Akamatsu et al., 2003; Candeias et al., 1996; Touvrey et al., 2006). We classified an imprecise SJ as aberrant if it carried a deletion, an insertion of genomic sequence or both. For Vδ5-Dδ2 SJs, which, unlike Vβ14-Dβ1 SJs, often exhibit small deletions in the wild-type setting (Touvrey et al., 2006), we further distinguished deletions of ≤ 7 bp from either end from those of ≥ 15 bp (Supplemental Table S1).

Of 102 Vβ14-Dβ1 SJs from wild-type (WT/WT and WT*/WT*) mice, 8 were imprecise as a consequence of N region addition (Fig. 3 and Supplemental Table S1). Of 60 Vβ14-Dβ1 SJs from T490A/T490A mice, 12 were imprecise. In contrast to the wild-type junctions, half of the imprecise SJs from mutant mice were aberrant (Fig. 3 and Supplemental Table S1). Of 143 *Vδ5-Dδ2* SJs from wild-type mice, 37 were imprecise; of these, 18 were classified as aberrant because of small (≤ 7 bp) deletions from one or both signal ends (Fig. 4A and Supplemental Table S1). Of 75 Vδ5-Dδ2 SJs from RAG-2(T490A) mutant mice, 21 were imprecise and 12 were classified as aberrant. The aberrant SJs from mutant mice differed from those of wild-type, however, in that 7 of 12 exhibited large deletions (≥ 15 bp), insertions corresponding to genomic sequence, or both. The insertions were apparently derived from adjacent coding flanks or non-adjacent genomic sequence (Fig. 4A and Supplemental Table S1). One 95-bp insertion was derived from the Jδ1 RSS and its 5′ flank; a 54-bp insertion contained a fusion between Dδ2 and the Vδ5 RSS, as well as partial tandem repeats of the Dδ2 12 RSS (Fig. 4A). Microhomology of greater than 1 bp was observed only twice in the 18 aberrant SJs obtained from mutant mice. These observations

suggest abnormal repair of recombinase-induced breaks by a mechanism involving classical, rather than alternative, NHEJ. Similar aberrations (Talukder et al., 2004) have been observed at SJs from mice carrying a truncation that removes the entire non-core region of RAG-2, which spans residues 387 through 527.

We also examined coding joints produced by inversional recombination between Vβ14 and Dβ1Jβ1 in mice expressing RAG-2(T490A). With respect to junctional modification and deletion from the J or D segment, these coding joints were similar to those from wild-type mice (Supplemental Fig. S3 and Supplemental Table S2). A small but significant increase in the average length of deletion from the V segment was observed in mice expressing RAG-2(T490A) (Supplemental Table S2), as has been documented in mice in which the RAG-2 non-core region is deleted (Talukder et al., 2004).

Mistargeted DNA cleavage by the mutant recombinase could formally account for some of the aberrant SJs from RAG-2(T490A) mice. To examine this we tested RAG-2(T490A) in an assay for DNA cleavage in vitro (Bergeron et al., 2006). In the presence of core RAG-1, wild-type RAG-2 and RAG-2(T490A) supported similar amounts of nicking and transesterification on 12-RSS and 23-RSS substrates; importantly, we observed no difference between wild-type and mutant RAG-2 with respect to off-target nicking or transesterification (Supplemental Fig. S4A). We also compared wild-type RAG-2 and RAG-2(T490A) in extrachromosomal assays for recombination and failed to observe a significant difference with respect to the frequency or fidelity of SJ formation (Supplemental Fig. S4B). Taken together these results suggest strongly that the aberrant features of SJs from RAG-2(T490A) mice are introduced after the appropriately targeted cleavage of endogenous gene segments.

Aberrant V(D)J recombination in mice lacking the Skp-2-SCF ubiquitin ligase

It remained possible that the effect of the T490A mutation on the repair of RAG-induced DNA breaks was independent of its effect on the periodic degradation of RAG-2. To address this we sought a setting in which accumulation of RAG-2 is relieved from cell cycle control without alteration of the RAG-2 protein itself. The Skp2-SCF E3 ubiquityl ligase is responsible for programmed destruction of RAG-2; thus, in Skp2-deficient thymocytes RAG-2 persists throughout the cell cycle (Jiang et al., 2005). We reasoned that if the aberrant SJs recovered from RAG-2(T490A)-expressing mice were the result of mistimed RAG activity, then an increase in the yield of aberrant recombination products would also be observed in Skp2-deficient mice.

We compared Vβ14-Dβ1 SJs from $Skp2^{+/-}$ and $Skp2^{-/-}$ thymocytes. No aberrant junctions were found among 68 Vβ14-Dβ1 SJ sequences recovered from $Skp2^{+/-}$ mice (Fig. 3 and Supplemental Table S3). In contrast, 14 of 33 Vβ14-Dβ1.1 SJ sequences recovered from $Skp2^{-/-}$ thymocytes were aberrant according to criteria defined above. We also examined Vδ5-Dδ2 SJs from $Skp2^{+/-}$ and $Skp2^{-/-}$ thymocytes. Of 77 Vδ5-Dδ2 signal sequences recovered from $Skp2^{+/-}$ thymocytes, 4 were aberrant because of small (≤ 7 bp) deletions from one or both signal ends (Fig. 4B and Supplemental Table S3). In contrast, among 125 Vδ5-Dδ2 signal sequences recovered from $Skp2^{-/-}$ thymocytes, 28 were aberrant; of these, 16 exhibited long deletions ranging from 15 bp to 295 bp at either end (Fig. 4B and Supplemental Table S3). In 2 aberrant sequences the Dδ2 coding sequence was represented intact and bounded at one end by potential P elements and N additions (Fig. 4B). No microhomology of greater than 1 bp was observed among the aberrant SJs from $Skp2^{-/-}$ mice, consistent with the infrequency of microhomology at SJs from RAG-2(T490A)-expressing animals. The difference in recovery of aberrant recombination products from $Skp2^{+/-}$ and $Skp2^{-/-}$ animals at TCRβ ($p < 0.0001$) and TCRδ ($p = 0.0012$) is highly

significant (Supplemental Table S3) and consistent with the interpretation that DNA breaks produced by RAG outside of G0-G1 are subject to non-canonical repair.

Unscheduled RAG activity is associated with lymphoid tumors bearing complex chromosomal translocations involving antigen receptor loci

The frequent aberrant rearrangement and increased apoptosis in mice expressing RAG-2(T490A) suggested that removal of p53 might unmask oncogenic effects of the RAG-2(T490A) mutation, by analogy to the effects of combined NHEJ and p53 deficiency. We introduced the *Rag2*(T490A) allele or the WT* allele onto a p53-deficient background. About half of the single-mutant (*Rag2*$^{wt*/wt*}$, *Trp53*$^{-/-}$ and *Rag2*$^{wt/wt}$, *Trp53*$^{-/-}$) mice developed T cell lymphomas by 20 weeks (Supplemental Fig. S5A), consistent with previous studies (Jacks et al., 1994). Double-mutant (*Rag2*$^{T490A/wt}$, *Trp53*$^{-/-}$ and *Rag2*$^{T490A/T490A}$, *Trp53*$^{-/-}$) mice exhibited a tumor latency similar to that of the p53-null animals, but with a distinctive tumor phenotype. The single-mutant, p53-null animals did not develop B lymphoid tumors (Supplemental Fig. S5B), whereas one fourth of the malignancies arising in RAG-2(T490A), p53-null mice were B lymphomas (Supplemental Fig. S5B and Table 1). Moreover, whereas T lymphomas from single-mutant, p53-deficient mice were $CD4^+CD8^+$, as expected (Jacks et al., 1994), most T lymphomas from double-mutant mice were of the less mature $CD4^-CD8^-$ or $CD4^-$CD8 intermediate single positive ($CD4^-$CD8 ISP) phenotypes (Table 1).

Spectral karyotypic analysis revealed robust differences between the lymphomas arising in the double-mutant mice and those associated with p53-deficiency alone. Lymphomas from p53-deficient mice rarely exhibit clonal chromosomal translocations (Haines et al., 2006). The T lymphomas from *Rag2*$^{wt/wt}$, *Trp53*$^{-/-}$ and *Rag2*$^{wt*/wt*}$, *Trp53*$^{-/-}$ mice were consistent with these observations (Fig. 5A; Table 1). In contrast, 7 of 8 lymphoid tumors analyzed from *Rag2*$^{T490A/wt}$, *Trp53*$^{-/-}$ and *Rag2*$^{T490A/T490A}$, *Trp53*$^{-/-}$ mice carried clonal chromosomal translocations (Fig. 5A; Table 1). In all 7 of these tumors, at least one translocation involved a chromosome carrying an antigen receptor locus. In most cases multiple clonal translocations were observed. Two T lymphomas carried complex clonal translocations (Table 1) and in one tumor more than one complex translocation was observed (Supplemental Fig. S5C).

Mapping of translocation breakpoints to antigen receptor loci in lymphomas from RAG-2(T490A) mutant mice

Rearrangements involving chromosome 14, which carries the TCRα and TCRδ locus, were found in all T lymphomas with clonal translocations (Table 1). We used chromosome painting and fluorescence in-situ hybridization (FISH) to localize the t(12;14) translocation breakpoint relative to the TCRα and TCRδ locus in tumor 2297, a T cell lymphoma from a p53-deficient, RAG-2(T490A) mutant mouse. As a reference we performed a similar analysis using tumor 2319, a polyploid T cell lymphoma derived from a p53-deficient mouse expressing wild-type RAG-2. In both tumors a probe specific for the TCRα and TCRδ locus hybridized to a site within intact chromosome 14, as expected (Fig. 5B). In the t(12;14) translocation of tumor 2297 the TCRα and TCRδ locus resided near the translocation boundary (Fig. 6B, bottom). Further analysis showed that the t(12;14) translocation in tumor 2297 splits the TCRα and TCRδ locus (Fig. 5C), as the translocation boundary was stained by a probe specific for the 3′ (red), but not the 5′ (green) region of the TCRα and TCRδ locus (Fig. 5C).

Rearrangements involving chromosome 12, which carries the IgH locus, were found in both B lymphomas that were analyzed by spectral karyotyping (Table 1). The $B220^+IgM^+IgD^+CD43^+$ tumor 2135 (Fig. 6A), which carries a t(12;16) translocation (Table

1), was analyzed by FISH. Probes specific for telomeric (5′, red) and centromeric (3′, green) regions of the IgH locus hybridized near each another in intact chromosome 12 (Fig. 6B). In contrast, the t(12;16) translocation was stained by the 3′-specific probe, but not by the 5′-specific probe (Fig. 6B), indicating that the translocation boundary splits the IgH locus. Moreover, the region stained by the 3′-specific probe was broader at the t(12;16) translocation than at the intact locus, indicating amplification near the translocation boundary (Fig. 6B, inset). Taken together, these observations suggest that persistence of RAG activity throughout cell cycle predisposes to aberrant V(D)J recombination and, in the context of p53-deficiency, to genomic instability and malignant transformation.

Discussion

Several lines of evidence implicate V(D)J recombination in the genesis of lymphoid tumors. First, chromosomal translocations involving antigen receptor loci and protooncogenes are often observed in human lymphomas (Marculescu et al., 2006). A subset of such translocations may arise from aberrant V(D)J recombination events, involving mistargeting of the recombinase to cryptic, non-consensus RSSs or joining of RAG-induced breaks to DNA ends created by other means, such as radiation (Marculescu et al., 2006). Second, impairment of NHEJ, in combination with p53 deficiency, promotes development of B cell lymphomas in mice (Difilippantonio et al., 2000; Gao et al., 2000; Zhu et al., 2002). These tumors typically exhibit clonal translocations involving the IgH locus and the *Myc* protooncogene, and apparently result from misrepair of RAG-induced DNA breaks (Difilippantonio et al., 2000; Gao et al., 2000; Zhu et al., 2002). In the absence of NHEJ the V(D)J recombinase can confer genomic instability even in the periphery (Wang et al., 2009). Third, double-strand break surveillance proteins, including ATM and H2AXγ, accumulate at sites of RSS cleavage and may suppress oncogenic translocations associated with V(D)J recombination (Bassing et al., 2003; Bredemeyer et al., 2006; Callen et al., 2007; Celeste et al., 2002; Chen et al., 2000; Perkins et al., 2002).

We have now shown that mutation of the cyclinA-CDK2 phosphorylation site within RAG-2, in combination with p53 deficiency, promotes the generation of B and T lymphomas. These tumors bear clonal chromosomal translocations whose breakpoints lie within antigen receptor loci. Mice expressing RAG-2(T490A) on a p53-deficient background developed lymphoid tumors that were phenotypically more mature than those from p53-null, NHEJ-deficient animals. This may be explained, at least in part, by the fact that in NHEJ-deficient mice lymphoid development is arrested at the pro-B and pro-T stages. The long latency of tumors from RAG-2(T490A), p53-deficient mice, relative to those associated with NHEJ-deficiency (Difilippantonio et al., 2000; Gao et al., 2000), may reflect the intactness of NHEJ in the RAG-2(T490A), p53-deficient animals.

The broad spectrum of chromosomal translocations in tumors from RAG-2(T490A), p53-deficient mice is reminiscent of that seen in human T-cell acute lymphoblastic leukemia (T-ALL). Translocations of the TCRα and TCRδ locus occur in about 20% of T-ALL tumors and involve at least 7 different recombination partners (Marculescu et al., 2006). The spectrum of translocations in tumors from RAG-2(T490A), p53-deficient mice was also broader than that seen in NHEJ-deficient, p53-deficient animals, which typically harbor one to a few dominant translocations (Difilippantonio et al., 2000; Gao et al., 2000; Zhu et al., 2002). The diversity of T lymphomas arising in RAG-2(T490A), p53-deficient mice suggest that the events initiating translocation in these animals may be more promiscuous and occur over a longer developmental interval than those in NHEJ-deficient, p53-deficient mice.

The high frequency of aberrant signal joining in RAG-2(T490A) mice is most easily explained by defective repair of RAG-induced DNA breaks, which may in turn underlie the

IgH and TCR translocations in lymphomas from these mice. These aberrant events are likely to result from the persistence of RAG activity throughout the cell cycle, because similarly aberrant SJs also accumulate in mice lacking Skp2, which mediates destruction of RAG-2 at the G1-S transition (Jiang et al., 2005). Several additional considerations argue that anomalous recombination in RAG-2(T490A)-expressing mice does not result from a change in the intrinsic activity of RAG-2. First, the T490A mutation had no discernable effect on the specificity of DNA cleavage in vitro. Second, failure to degrade RAG-2(T490A) at the G1-S transition is unlikely to hinder repair because wild-type RAG-2 and RAG-2(T490A) support SJ formation with similar efficiency. Third, while the T490A mutation could have impaired an interaction of RAG with NHEJ components, the ability of Skp2 deficiency to phenocopy RAG-2(T490A) with respect to aberrant joining argues that loss of programmed RAG-2 degradation is responsible for this phenotype.

There are at least two ways to explain the appearance of signal ends in S-G2-M phase thymocytes from RAG-2(T490A) mice: (1) de novo DNA cleavage outside of G0-G1 and (2) carryover of ends from G0-G1 because of a failure to degrade RAG-2. The two possibilities are not mutually exclusive. The presence of inversional signal ends, which must be joined to avoid cell cycle arrest, apoptosis or chromosome loss, may provide indirect evidence for de novo cleavage in S-G2-M. Nonetheless, if programmed degradation of RAG-2 plays a role in disassembly of signal end complexes, the T490A mutation may promote carryover of signal ends into S-G2-M, particularly because signal end complexes are more stable than complexes containing coding ends.

The RAG-2 degradation signal lies within the 140-residue non-core region, which is dispensable for DNA cleavage *in vitro*. Wholesale deletion of the non-core region is associated with reduced efficiency of recombination (Cuomo and Oettinger, 1994; Kirch et al., 1998; McMahan et al., 1997; Sadofsky et al., 1994; Sadofsky et al., 1993; Steen et al., 1999), impaired V_H-to-DJ_H joining (Akamatsu et al., 2003; Kirch et al., 1998; Liang et al., 2002), increased production of hybrid joints (Sekiguchi et al., 2001), aberrant signal joining (Talukder et al., 2004), disordered rearrangement (Curry and Schlissel, 2008) and imprecise selection of cleavage sites (Curry and Schlissel, 2008). The mechanisms underlying these effects have remained unclear and are likely to be complex, because the non-core region subsumes several functions in addition to degradation, including interaction with modified chromatin (Liu et al., 2007; Matthews et al., 2007) and nuclear import (Ross et al., 2003). We infer that the aberrant junctions associated with deletion of the non-core region (Talukder et al., 2004), which resemble those from RAG-2(T490A) and *Skp2*$^{-/-}$ mice, result from a failure to destroy RAG-2 at the G1-S transition.

Some translocation junctions from human lymphomas involve the joining of RSS ends to non-RSS-mediated breaks (Marculescu et al., 2006). These junctions and similar ones modeled in cell culture (Lieber et al., 2006) often contain templated insertions, or T nucleotides, that appear to have been copied from sites at or near the participating DNA ends. Some insertions at aberrant SJs from RAG-2(T490A) or *Skp2*$^{-/-}$ mice also contain apparent T nucleotides. The presence of tandem duplications at several of these junctions suggests involvement of a replicative mechanism such as break-induced replication (BIR).

Two junctions from *Skp2*$^{-/-}$ mice include a Dδ2 coding sequence, flanked on one end by an apparent P element, an N region and the Vδ5 RSS. While these insertions could have been formed by templated synthesis, the presence of a P element is consistent with RAG-mediated cleavage and suggests two alternative ways in which the Dδ insertion could have been formed. One mechanism, consistent with the 12–23 rule, would involve Vδ5-to-Dδ1 joining, followed by a secondary rearrangement between the retained Vδ5-Dδ1 SJ and Dδ2. Another mechanism would invoke recombination between the 3′ RSS of Vδ5 and the 3′ RSS

of Dδ2, in violation of the 12–23 rule. Secondary rearrangement of retained SJs and violations of 12–23 joining have both been observed at the TCRδ locus (Carroll et al., 1993).

Aberrant SJs were more frequently recovered from Skp2-deficient mice than from RAG-2(T490A) mice. This need not imply a distinction in cleavage or repair, as antigen receptor loci themselves differ with respect to the frequency of aberrant joining. While Skp2-deficient mice exhibit specific cell cycle defects, including G1-to-S delay (Nakayama et al., 2000), impairment of the G2-to-M transition and endoduplication (Nakayama et al., 2000; Nakayama et al., 2004), no effects on DNA repair have been reported. Skp2-deficiency is not known to increase the frequency of lymphoid tumors. While it would be reasonable to expect Skp2 deficiency to promote lymphomagenesis on a p53-null background, any pro-lymphomagenic effect may be mitigated by the debilitating effect of Skp2 deficiency on cell cycle progression.

Periodic destruction of RAG-2 may temporally sequester V(D)J recombination intermediates from HR, by restricting DNA cleavage to times at which HR is minimally active (Takata et al., 1998). The T nucleotides associated with RSS-mediated chromosomal translocations have been proposed to involve the combined actions of NHEJ and abortive HR (Marculescu et al., 2006). If this is true, then a breakdown in the segregation of RAG-induced DNA breaks from HR might increase the frequency of such events. Persistent RAG activity could produce RSS ends at times when HR is active and when potential templates for repair are present as sister chromatids. Under these conditions RAG-induced double-strand breaks would remain available to NHEJ but could also be acted upon by factors associated with HR. Repair of RAG-induced DNA breaks through a combination of NHEJ and mechanisms associated with HR (Marculescu et al., 2006), such as BIR (Zhang et al., 2009), may explain the SJ aberrations seen in RAG-2(T490A) and Skp2-deficient mice. The rarity of such events in wild-type mice is consistent with a model in which restriction of V(D)J recombinase activity to the G1 cell cycle phase isolates RAG-induced DNA breaks from unproductive pathways of repair.

Experimental Procedures

Assay for V(D)J Recombination Intermediates

Genomic DNA was prepared from thymocytes of 7 – 10 d old mice, sorted into fractions of 2C or >2C DNA content as described (Li et al., 1996). Double-strand breaks at recombination signal sequences were detected by ligation-mediated PCR (Schlissel et al., 1993) and products were detected by hybridization to locus-specific oligonucleotide probes. For details see Supplemental Methods.

Spectral karyotyping and fluorescence *in situ* hybridization

Tumor cells were maintained in culture for 48 – 72 h and metaphase arrest was induced by colcemid. After fixation cells were dropped onto slides to obtain chromosome spreads. Spectral karyotyping (SKY) and single chromosome painting were performed with commercial fluorescent probes (SKYPaint, Applied Spectral Imaging). Mouse BAC clones corresponding to the 5′ and 3′ ends of the TCRα and TCRδ or IgH locus were used as probes for fluorescence *in situ* hybridization (FISH). For details see Supplemental Methods.

Analysis of recombinant signal junctions

Vβ14-Dβ1 signal joints (SJs) were amplified from thymocyte genomic DNA using the primers Vβ14SIGNAL and Dβ1.1SIGNAL (Talukder et al., 2004); Vδ5-Dδ2 SJs were amplified from RAG-2(T490A) mice with primers SR1 and SR2 (Talukder et al., 2004) and from Skp2-deficient mice with nested primers TCRVδ5A and TCRDδ2B (outside) and

TCRVδ5C and TCRDδ2D (inside). The sequences of these primers are given in Supplemental Methods. Amplicons were introduced into plasmid pCR2.1-TOPO by TA cloning (Invitrogen) and propagated in *E. coli*; individual colonies were selected for analysis. Precise SJs were identified by digestion with *Apa*LI. Imprecise, *Apa*LI-resistant junctions were analyzed further by nucleotide sequencing.

In vitro DNA cleavage assays

RAG fusion proteins were purified by amylose affinity chromatography as described (Bergeron et al., 2006). DNA cleavage reactions were performed in Mg^{2+} using the 12-RSS substrate DAR39/DAR40 or the 23-RSS substrate DAR61/DAR62 as described (Bergeron et al., 2006) except that core RAG-1 and full-length RAG-2 or RAG-2(T490A) were added at 200 ng each and HMG1 was added to a concentration of 4 μg/ml. Reactions were carried out at 37°C for the indicated times. Reaction products were fractionated by electrophoresis through a 15% denaturing polyacrylamide gel and detected with a phosphorimager.

Extrachromosomal recombination assays

Assays were performed as described (Hesse et al., 1987) with slight modification. Briefly, plasmids (10 μg) encoding MBP-RAG-1-myc-His and RAG-2 or RAG-2(T490A) were cotransfected with 4 μg pJH200 (Lieber et al., 1988) into NIH3T3 cells using Lipofectamine 2000 (Invitrogen). Plasmid DNA was isolated 40 – 48 hr after transfection using a miniprep kit (Qiagen). *E. coli* DH5α was transformed with 1 μ LB agar containing 50 μg/ml ampicillin; the remainder was plated on LB agar containing 50 μg/ml ampicillin and 12.5 μg/ml chloramphenicol. Plates were scored after 14 – 16 hr at 37 C.

Gene targeting, generation of mutant mice, antibodies and flow cytometry, elutriation of neonatal thymocytes, statistical analysis, oligonucleotides

See Supplemental Methods.

Supplementary Material

Refer to Web version on PubMed Central for supplementary material.

Acknowledgments

We are grateful to Drs. Carol Greider and Frederick Alt for the gift of BAC clones and to Dr. Keiichi Nakayama for Skp2-deficient mice. We thank Margaret Strong for advice, Ada Tam for cell sorting and Dominic Dordai and Nancy Platek for expert technical assistance. This work was supported by a grant from the National Cancer Institute and by a gift to the Institute for Cell Engineering.

References

Ahnesorg P, Smith P, Jackson SP. XLF interacts with the XRCC4-DNA ligase IV complex to promote DNA nonhomologous end-joining. Cell. 2006; 124:301–313. [PubMed: 16439205]

Akamatsu Y, Monroe R, Dudley DD, Elkin SK, Gartner F, Talukder SR, Takahama Y, Alt FW, Bassing CH, Oettinger MA. Deletion of the RAG2 C terminus leads to impaired lymphoid development in mice. Proc Natl Acad Sci U S A. 2003; 100:1209–1214. [PubMed: 12531919]

Bassing CH, Suh H, Ferguson DO, Chua KF, Manis J, Eckersdorff M, Gleason M, Bronson R, Lee C, Alt FW. Histone H2AX: a dosage-dependent suppressor of oncogenic translocations and tumors. Cell. 2003; 114:359–370. [PubMed: 12914700]

Bergeron S, Anderson DK, Swanson PC. RAG and HMGB1 proteins: purification and biochemical analysis of recombination signal complexes. Methods Enzymol. 2006; 408:511–528. [PubMed: 16793390]

Bredemeyer AL, Sharma GG, Huang CY, Helmink BA, Walker LM, Khor KC, Nuskey B, Sullivan KE, Pandita TK, Bassing CH, Sleckman BP. ATM stabilizes DNA double-strand-break complexes during V(D)J recombination. Nature. 2006; 442:466–470. [PubMed: 16799570]

Buck D, Malivert L, de Chasseval R, Barraud A, Fondaneche MC, Sanal O, Plebani A, Stephan JL, Hufnagel M, le Deist F, et al. Cernunnos, a novel nonhomologous end-joining factor, is mutated in human immunodeficiency with microcephaly. Cell. 2006; 124:287–299. [PubMed: 16439204]

Callen E, Jankovic M, Difilippantonio S, Daniel JA, Chen HT, Celeste A, Pellegrini M, McBride K, Wangsa D, Bredemeyer AL, et al. ATM prevents the persistence and propagation of chromosome breaks in lymphocytes. Cell. 2007; 130:63–75. [PubMed: 17599403]

Candeias S, Muegge K, Durum SK. Junctional diversity in signal joints from T cell receptor beta and delta loci via terminal deoxynucleotidyl transferase and exonucleolytic activity. J Exp Med. 1996; 184:1919–1926. [PubMed: 8920879]

Carroll AM, Slack JK, Mu X. V(D)J recombination generates a high frequency of nonstandard TCR Dδ-associated rearrangements in thymocytes. J Immunol. 1993; 150:2222–2230. [PubMed: 8383718]

Celeste A, Petersen S, Romanienko PJ, Fernandez-Capetillo O, Chen HT, Sedelnikova OA, Reina-San-Martin B, Coppola V, Meffre E, Difilippantonio MJ, et al. Genomic instability in mice lacking histone H2AX. Science. 2002; 296:922–927. [PubMed: 11934988]

Chen HT, Bhandoola A, Difilippantonio MJ, Zhu J, Brown MJ, Tai X, Rogakou EP, Brotz TM, Bonner WM, Ried T, Nussenzweig A. Response to RAG-mediated VDJ cleavage by NBS1 and gamma-H2AX. Science. 2000; 290:1962–1965. [PubMed: 11110662]

Corneo B, Wendland RL, Deriano L, Cui X, Klein IA, Wong SY, Arnal S, Holub AJ, Weller GR, Pancake BA, et al. RAG mutations reveal robust alternative end joining. Nature. 2007; 449:483–486. [PubMed: 17898768]

Cuomo CA, Oettinger MA. Analysis of regions of RAG-2 important for V(D)J recombination. Nucleic Acids Res. 1994; 22:1810–1814. [PubMed: 8208604]

Curry JD, Schlissel MS. RAG2's non-core domain contributes to the ordered regulation of V(D)J recombination. Nucl Acids Res. 2008; 36:5750–5762. [PubMed: 18776220]

Desiderio S, Lin WC, Li Z. The cell cycle and V(D)J recombination. Curr Top Microbiol Immunol. 1996; 217:45–59. [PubMed: 8787617]

Difilippantonio MJ, Zhu J, Chen HT, Meffre E, Nussenzweig MC, Max EE, Ried T, Nussenzweig A. DNA repair protein Ku80 suppresses chromosomal aberrations and malignant transformation. Nature. 2000; 404:510–514. [PubMed: 10761921]

Fugmann SD, Lee AI, Shockett PE, Villey IJ, Schatz DG. The RAG proteins and V(D)J recombination: complexes, ends, and transposition. Annu Rev Immunol. 2000; 18:495–527. [PubMed: 10837067]

Fukushima T, Takata M, Morrison C, Araki R, Fujimori A, Abe M, Tatsumi K, Jasin M, Dhar PK, Sonoda E, et al. Genetic analysis of the DNA-dependent protein kinase reveals an inhibitory role of Ku in late S-G2 phase DNA double-strand break repair. J Biol Chem. 2001; 276:44413–44418. [PubMed: 11577093]

Gao Y, Ferguson DO, Xie W, Manis JP, Sekiguchi J, Frank KM, Chaudhuri J, Horner J, DePinho RA, Alt FW. Interplay of p53 and DNA-repair protein XRCC4 in tumorigenesis, genomic stability and development. Nature. 2000; 404:897–900. [PubMed: 10786799]

Gellert M. V(D)J recombination: RAG proteins, repair factors, and regulation. Annu Rev Biochem. 2002; 71:101–132. [PubMed: 12045092]

Haines BB, Ryu CJ, Chang S, Protopopov A, Luch A, Kang YH, Draganov DD, Fragoso MF, Paik SG, Hong HJ, et al. Block of T cell development in P53-deficient mice accelerates development of lymphomas with characteristic RAG-dependent cytogenetic alterations. Cancer Cell. 2006; 9:109–120. [PubMed: 16473278]

Hesse JE, Lieber MR, Gellert M, Mizuuchi K. Extrachromosomal DNA substrates in pre-B cells undergo inversion or deletion at immunoglobulin V-(D)-J joining signals. Cell. 1987; 49:775–783. [PubMed: 3495343]

Jacks T, Remington L, Williams BO, Schmitt EM, Halachmi S, Bronson RT, Weinberg RA. Tumor spectrum analysis in p53-mutant mice. Curr Biol. 1994; 4:1–7. [PubMed: 7922305]

Jiang H, Chang FC, Ross AE, Lee J, Nakayama K, Nakayama K, Desiderio S. Ubiquitylation of RAG-2 by Skp2-SCF links destruction of the V(D)J recombinase to the cell cycle. Mol Cell. 2005; 18:699–709. [PubMed: 15949444]

Jiang H, Ross AE, Desiderio S. Cell cycle-dependent accumulation in vivo of transposition-competent complexes between recombination signal ends and full-length RAG proteins. J Biol Chem. 2004; 279:8478–8486. [PubMed: 14660558]

Kirch SA, Rathbun GA, Oettinger MA. Dual role of RAG2 in V(D)J recombination: catalysis and regulation of ordered Ig gene assembly. Embo J. 1998; 17:4881–4886. [PubMed: 9707447]

Lee GS, Neiditch MB, Salus SS, Roth DB. RAG proteins shepherd double-strand breaks to a specific pathway, suppressing error-prone repair, but RAG nicking initiates homologous recombination. Cell. 2004; 117:171–184. [PubMed: 15084256]

Lee J, Desiderio S. Cyclin A/CDK2 regulates V(D)J recombination by coordinating RAG-2 accumulation and DNA repair. Immunity. 1999; 11:771–781. [PubMed: 10626899]

Li Z, Dordai DI, Lee J, Desiderio S. A conserved degradation signal regulates RAG-2 accumulation during cell division and links V(D)J recombination to the cell cycle. Immunity. 1996; 5:575–589. [PubMed: 8986717]

Liang HE, Hsu LY, Cado D, Cowell LG, Kelsoe G, Schlissel MS. The “dispensable” portion of RAG2 is necessary for efficient V-to-DJ rearrangement during B and T cell development. Immunity. 2002; 17:639–651. [PubMed: 12433370]

Lieber MR, Hesse JE, Lewis S, Bosma GC, Rosenberg N, Mizuuchi K, Bosma MJ, Gellert M. The defect in murine severe combined immune deficiency: joining of signal sequences but not coding segments in V(D)J recombination. Cell. 1988; 55:7–16. [PubMed: 3167977]

Lieber MR, Ma Y, Pannicke U, Schwarz K. Mechanism and regulation of human non-homologous DNA end-joining. Nat Rev Mol Cell Biol. 2003; 4:712–720. [PubMed: 14506474]

Lieber MR, Yu K, Raghavan SC. Roles of nonhomologous DNA end joining, V(D)J recombination, and class switch recombination in chromosomal translocations. DNA Repair (Amst). 2006; 5:1234–1245. [PubMed: 16793349]

Lin WC, Desiderio S. Regulation of V(D)J recombination activator protein RAG-2 by phosphorylation. Science. 1993; 260:953–959. [PubMed: 8493533]

Lin WC, Desiderio S. Cell cycle regulation of V(D)J recombination- activating protein RAG-2. Proc Natl Acad Sci U S A. 1994; 91:2733–2737. [PubMed: 8146183]

Liu Y, Subrahmanyam R, Chakraborty T, Sen R, Desiderio S. A plant homeodomain in RAG-2 that binds hypermethylated lysine 4 of histone H3 is necessary for efficient antigen-receptor-gene rearrangement. Immunity. 2007; 27:561–571. [PubMed: 17936034]

Marculescu R, Vanura K, Montpellier B, Roulland S, Le T, Navarro JM, Jager U, McBlane F, Nadel B. Recombinase, chromosomal translocations and lymphoid neoplasia: targeting mistakes and repair failures. DNA Repair (Amst). 2006; 5:1246–1258. [PubMed: 16798110]

Matthews A, Kuo A, Ramón-Maiques S, Han S, Champagne K, Ivanov D, Gallardo M, Carney D, Cheung P, Ciccone D, Walter K, Utz P, Shi Y, Kutateladze T, Yang W, Gozani O, Oettinger M. RAG-2 PHD finger couples histone H3 lysine 4 trimethylation with V(D)J recombination. Nature. 2007; 450:1106–1110. [PubMed: 18033247]

McMahan CJ, Difilippantonio MJ, Rao N, Spanopoulou E, Schatz DG. A basic motif in the N-terminal region of RAG1 enhances V(D)J recombination activity. Mol Cell Biol. 1997; 17:4544–4552. [PubMed: 9234712]

Nakayama K, Nagahama H, Minamishima YA, Matsumoto M, Nakamichi I, Kitagawa K, Shirane M, Tsunematsu R, Tsukiyama T, Ishida N, et al. Targeted disruption of Skp2 results in accumulation of cyclin E and p27(Kip1), polyploidy and centrosome overduplication. EMBO J. 2000; 19:2069–2081. [PubMed: 10790373]

Nakayama K, Nagahama H, Minamishima YA, Miyake S, Ishida N, Hatakeyama S, Kitagawa M, Iemura S, Natsume T, Nakayama KI. Skp2-mediated degradation of p27 regulates progression into mitosis. Dev Cell. 2004; 6:661–672. [PubMed: 15130491]

Perkins EJ, Nair A, Cowley DO, Van Dyke T, Chang Y, Ramsden DA. Sensing of intermediates in V(D)J recombination by ATM. Genes Dev. 2002; 16:159–164. [PubMed: 11799059]

Ross A, Vuica M, Desiderio S. Overlapping signals for protein degradation and nuclear localization define a role for intrinsic RAG-2 nuclear uptake in dividing cells. Mol Cell Biol. 2003; 23:5308–5319. [PubMed: 12861017]

Sadofsky MJ, Hesse JE, Gellert M. Definition of a core region of RAG-2 that is functional in V(D)J recombination. Nucleic Acids Res. 1994; 22:1805–1809. [PubMed: 8208603]

Sadofsky MJ, Hesse JE, McBlane JF, Gellert M. Expression and V(D)J recombination activity of mutated RAG-1 proteins. Nucleic Acids Res. 1993; 21:5644–5650. [PubMed: 8284210]

Sekiguchi JA, Whitlow S, Alt FW. Increased accumulation of hybrid V(D)J joins in cells expressing truncated versus full-length RAGs. Mol Cell. 2001; 8:1383–1390. [PubMed: 11779512]

Schlissel M, Constantinescu A, Morrow T, Baxter M, Peng A. Double-strand signal sequence breaks in V(D)J recombination are blunt, 5′-phosphorylated, RAG-dependent, and cell cycle regulated. Genes Dev. 1993; 7:2520–2532. [PubMed: 8276236]

Steen SB, Han JO, Mundy C, Oettinger MA, Roth DB. Roles of the “dispensable” portions of RAG-1 and RAG-2 in V(D)J recombination. Mol Cell Biol. 1999; 19:3010–3017. [PubMed: 10082568]

Takata M, Sasaki MS, Sonoda E, Morrison C, Hashimoto M, Utsumi H, Yamaguchi-Iwai Y, Shinohara A, Takeda S. Homologous recombination and non-homologous end-joining pathways of DNA double-strand break repair have overlapping roles in the maintenance of chromosomal integrity in vertebrate cells. EMBO J. 1998; 17:5497–5508. [PubMed: 9736627]

Talukder SR, Dudley DD, Alt FW, Takahama Y, Akamatsu Y. Increased frequency of aberrant V(D)J recombination products in core RAG-expressing mice. Nucleic Acids Res. 2004; 32:4539–4549. [PubMed: 15328366]

Touvrey C, Borel E, Marche PN, Jouvin-Marche E, Candeias SM. Gene-specific signal joint modifications during V(D)J recombination of TCRAD locus genes in murine and human thymocytes. Immunobiology. 2006; 211:741–751. [PubMed: 17015149]

Wang JH, Gostissa M, Yan CT, Goff P, Hickernell T, Hansen E, Difilippantonio S, Wesemann DR, Zarrin AA, Rajewsky K, et al. Mechanisms promoting translocations in editing and switching peripheral B cells. Nature. 2009; 460:231–236. [PubMed: 19587764]

Zhang F, Carvalho CMB, Lupski JR. Complex human chromosomal and genomic rearrangements. Trends Genet. 2009; 25:298–307. [PubMed: 19560228]

Zhu C, Mills KD, Ferguson DO, Lee C, Manis J, Fleming J, Gao Y, Morton CC, Alt FW. Unrepaired DNA breaks in p53-deficient cells lead to oncogenic gene amplification subsequent to translocations. Cell. 2002; 109:811–821. [PubMed: 12110179]

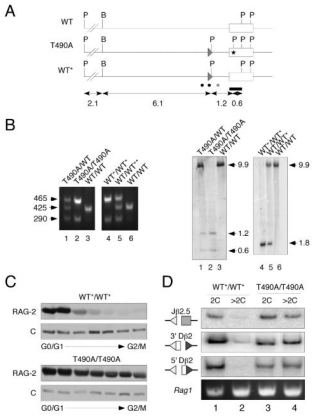

Figure 1.

Uncoupling of V(D)J recombination from cell cycle in *Rag2*(T490A) knockin mice. (A) Generation of *Rag2*(T490A) knockin mice. Top, wild-type *Rag2* allele (wt); middle, neo-excised *Rag2*(T490A) allele (T490A); bottom, neo-excised, wild-type *Rag2* allele (WT*). Open box, *Rag2* coding exon. Direction of transcription is right to left. Filled triangle, *loxP* site; P, *Pst*I; B, *Bam*HI; asterisk, location of nucleotide substitutions specifying the T490A mutation and a novel *Pst*I restriction site. Bar, probe used to assay recombinants by Southern hybridization. Dots below indicate positions of forward (black) and reverse (gray) PCR primers used for genotyping. Sizes of restriction fragments, in kb, are indicated below. (B) Assay for wild-type (WT), neo-excised wild-type (WT*) and neo-excised mutant (T490A) alleles. Genomic DNA was screened by PCR (left panels) with primers indicated in (A). Sizes of amplicons are indicated in bp. Genotypes were confirmed by Southern hybridization (right panels). Genomic DNA was digested with *Pst*I and hybridized to the probe indicated in (A). Sizes of products are indicated in kb. (C) Cell cycle independence of RAG-2 accumulation in RAG-2 T490A mice. Thymocytes from wt*/wt* or T490/T490A mice were fractionated by centrifugal elutriation. Progression from 2C (G0-G1) to 4C (G2-M) DNA content is indicated below. Fractions were assayed for RAG-2 by immunoblotting. C, invariant, cross reactive species, used as an internal control. (D) Accumulation of RSS breaks is uncoupled from cell cycle in RAG-2(T490A) mice. Thymocytes from neo-excised wild-type (WT*/WT*) or mutant (T490A/T490A) mice were sorted into fractions of 2C or >2C DNA content. Double-strand DNA breaks at Jβ2.5, 3′Dβ2 and 5′Dβ2 RSSs (indicated at left) were assayed by LM-PCR amplification of genomic DNA. A portion of the *Rag1* gene was amplified in parallel to monitor the amounts of genomic DNA in each reaction.

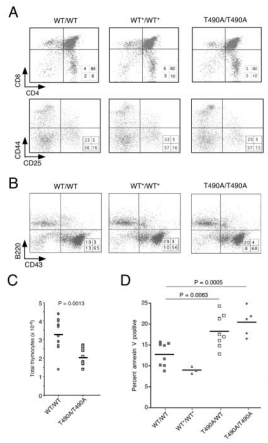

Figure 2.

Analysis of lymphoid lineages in RAG-2(T490A) mice. (A) Flow cytometric analysis of thymocytes from homozygous RAG-2 wild-type (WT/WT), *neo*-excised RAG-2 wild-type (WT*/WT*) and RAG-2(T490A) (T490A/T490A) mice. Upper panel, thymocytes assayed for CD4 and CD8; lower panel, thymocytes, gated on the $CD4^{-}CD8^{-}$ population, assayed for CD44 and CD25. (B) Flow cytometric analysis of bone marrow cells, assayed for B220 and CD43, from homozygous RAG-2 wild-type (wt/wt), *neo*-excised RAG-2 wild-type (wt*/wt*) and RAG-2 T490A (T490A/T490A) mice. Percentages of cells within each quadrant are indicated. (C) Reduction of thymic cellularity in homozygous RAG-2 T490A mice, relative to wild-type. Circles (wt/wt) and squares (T490A/T490A) represent cellularity of thymuses from individual mice; horizontal bars indicate mean cellularity. Significance was estimated by the two-tailed t test. (D) Increased apoptosis among $CD4^{-}CD8^{-}$ thymocytes from RAG-2 T490A mice. Symbols represent individual mice; horizontal bars indicate mean percentages. Genotypes are indicated in inset at right. Significant differences are indicated with confidence limits as determined by the two-tailed t test.

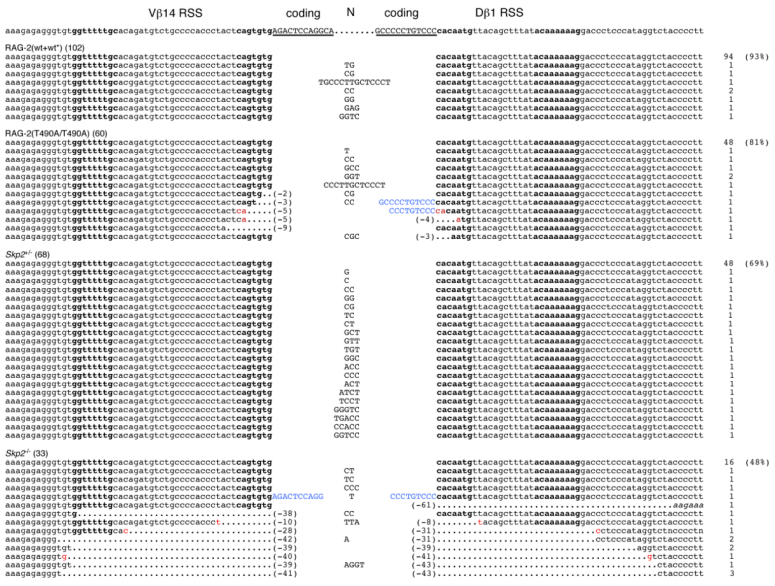

Figure 3.

Increased recovery of aberrant Vβ14-Dβ1 signal joints from mice expressing RAG-2(T490A) or deficient in Skp2. Top, Vβ14 and Dβ1 RSSs and flanking coding sequences. Heptamer and nonomer elements are indicated in boldface; coding sequences are underlined and capitalized. In each sequence below, the RSSs are in lowercase and insertions in uppercase. Sets of sequences from RAG-2 wild-type, RAG-2(T490A), *Skp2*$^{+/-}$ and *Skp2*$^{-/-}$ animals are indicated. Nucleotide additions of more than three contiguous bases identical to either coding flank are capitalized in blue. The sizes of deletions from each signal end, in bp, are given in parentheses. Potential microhomologies are indicated in red type. The number of junctions obtained for a given sequence is indicated at right.

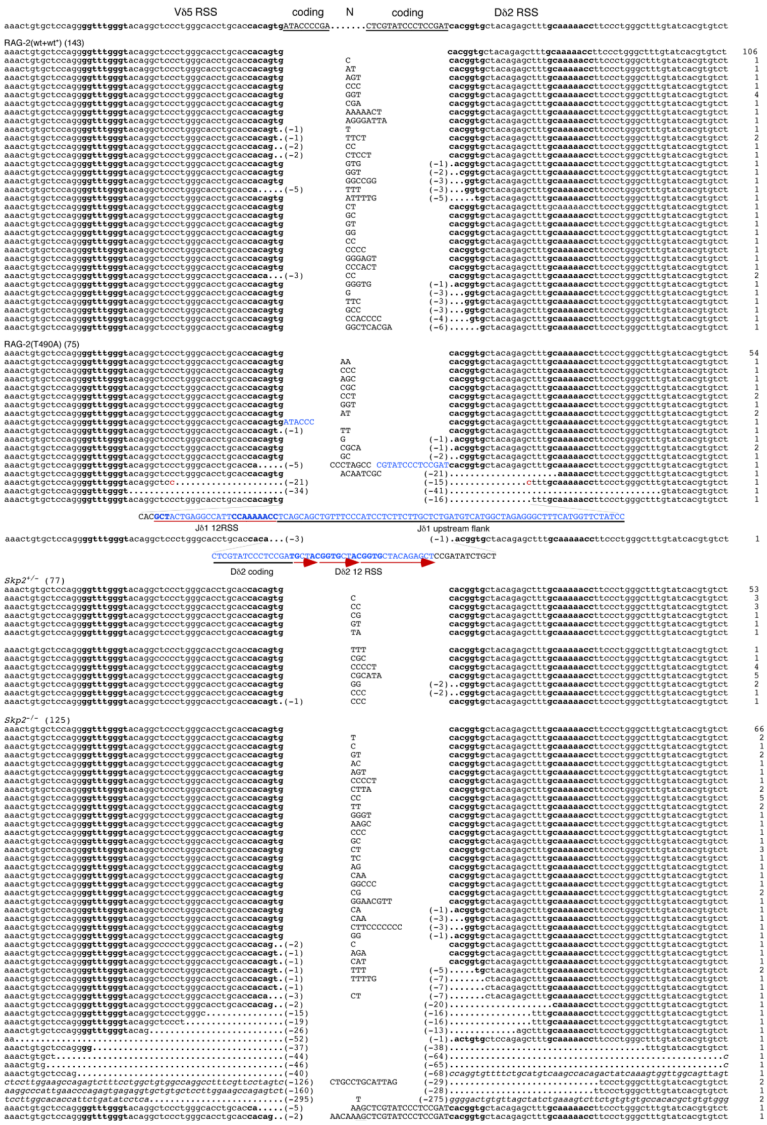

Figure 4.

Increased recovery of aberrant Vδ5-Dδ2 signal joints from mice expressing RAG-2(T490A) or deficient in Skp2. (A) Comparison of *Vδ5-Dδ2* SJs from wild-type and RAG-2(T490A) knockin mice. Top, Vδ5 and Dδ2 RSSs and flanking coding sequences, annotated as in Fig. 3. Deletions, potential microhomologies and numbers of isolates are designated as in Fig. 3. Insertions corresponding to flanking coding sequence or to other genomic sequence are indicated in capitals and blue type. The presence of a partial Jδ1 RSS within one junctional insertion is designated by a red underline. A portion of the Jδ1 upstream flank within the same insertion is underlined in black. In a separate junctional insertion, a complete Dδ2 coding sequence is underlined in black and partial tandem repeats of the Dδ2 12 RSS are underscored by red arrows. (B) Comparison of Vδ5-Dδ2 SJs from *Skp2*$^{+/-}$ and *Skp2*$^{-/-}$ mice. Top, Vδ5 and Dδ2 RSSs and flanking coding sequences, annotated as in Fig. 3. Deletions, potential microhomologies and numbers of isolates are designated as in Fig. 3. Italics denote sequences surrounding deletions whose endpoints lie beyond the reference shown at top. Insertions corresponding to flanking coding sequence are indicated in capitals and blue type; potential P elements are underlined.

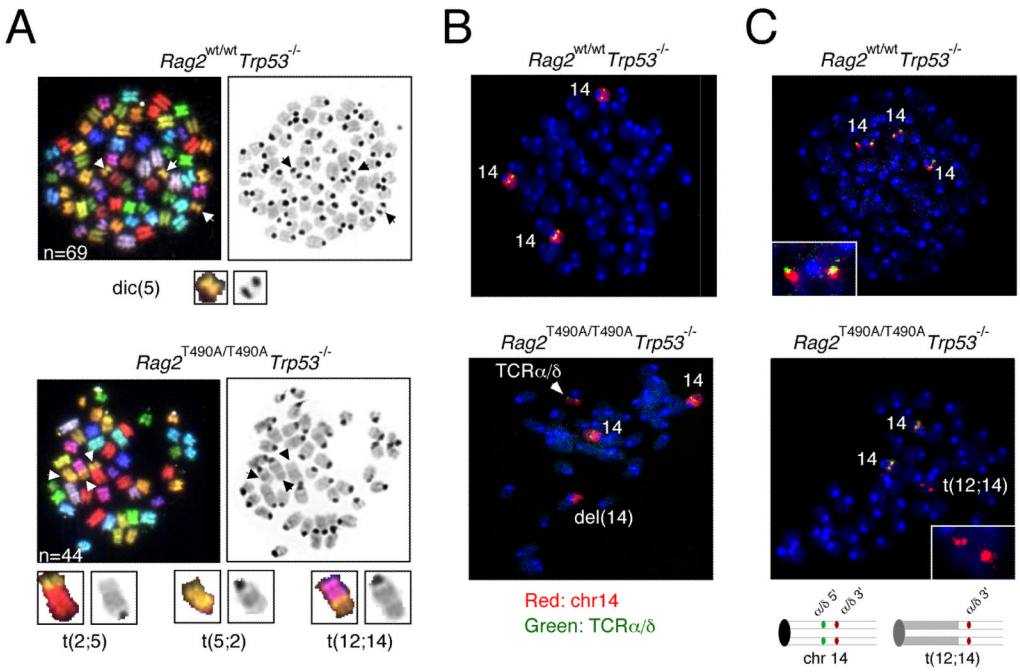

Figure 5.

A t(12;14) translocation splits the TCRα and TCRδ locus in a T cell lymphoma from a p53-deficient, RAG-2 T490A mouse. (A) Spectral karyotypic (SKY) analysis of metaphase chromosomes from tumor 2319 (*Rag2*$^{wt/wt}$*Trp53*$^{-/-}$; upper panels) or tumor 2297 (*Rag2*$^{T490A/T490A}$*Trp53*$^{-/-}$; lower panels). SKY images are shown at left and DAPI-stained images at right. Arrows, aberrant chromosomes; n, ploidy. Enlarged images of each aberrant chromosome are given below; chromosomal origins are indicated; t, translocation; dic, dicentric. The karyotypic analyses of all tumors examined in this study are summarized in Table 1. (B) Translocation breakpoint of t(12;14) translocation in tumor 2297 lies at or near the TCRα and TCRδ locus. Fluorescence *in situ* hybridization (FISH) to metaphase chromosome spreads from *Rag2*$^{wt/wt}$*Trp53*$^{-/-}$ tumor 2319 (upper panel) or *Rag2*$^{T490A/T490A}$*Trp53*$^{-/-}$ tumor 2297 (lower panel) using a TCRα and TCRδ-specific probe (green) and a chromosome 14-specific probe (red). Normal chromosomes 14 (14), the deleted portion of chromosome 14 (del[14]) and the position of the TCRα and TCRδ locus are indicated. (C) The t(12;14) translocation breakpoint in tumor 2297 lies within the TCRα and TCRδ locus. FISH was performed against metaphase chromosome spreads from *Rag2*$^{wt/wt}$*Trp53*$^{-/-}$ tumor 2319 (upper panel) or *Rag2*$^{T490A/T490A}$*Trp53*$^{-/-}$ tumor 2297 (lower panel) using probes specific for the 5′ (green) or 3′ (red) regions of the TCR α and TCRδ locus. The inset in the upper panel represents an enlarged image of intact chromosome 14, exhibiting superimposed signals from 5′ and 3′ probes. The inset in the lower panel represents an enlarged image of the t(12;14) translocation, which hybridized only to the 3′ probe. The deduced arrangements of hybridized probes in intact chromosome 14 and the t(12;14) translocation are diagrammed below.

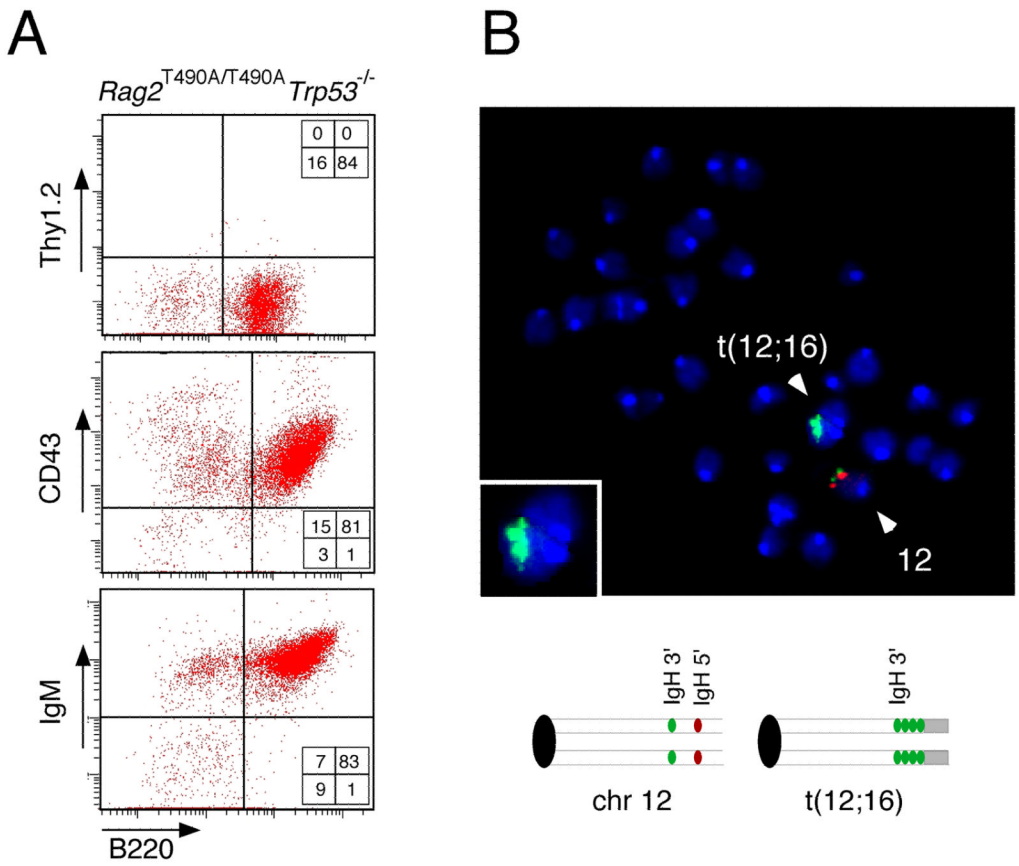

Figure 6.

A t(12;16) translocation splits and amplifies a portion of the IgH locus in a B cell lymphoma from a p53-deficient, RAG-2 T490A mouse. (A) Flow cytometric analysis of tumor 2135 (*Rag2*$^{T490A/T490A}$*Trp53*$^{-/-}$) indicates a tumor of B lymphoid origin. Dispersed tumor cells were stained for the surface markers B220 and Thy1.2 (top), CD43 (middle) and IgM (bottom). (B) Analysis of a metaphase spread from the same tumor by FISH using BAC probes specific for the 5′ flank of the IgH locus (red) and the 3′ flank of the IgH locus (green). Inset represents an enlarged image of t(12;16), which had been detected by SKY analysis (see Table 1). The deduced arrangements of probes in intact chromosome12 and the t(12;16) translocation are indicated below.

Table 1

Clonal translocations in lymphoid tumors from p53-deficient, RAG-2(T490A) mutant mice

Clonal chromosomal translocations in lymphoid tumors from p53-deficient, RAG-2(T490A) mutant mice. For each tumor the genotype of origin, lineage and cell surface phenotype are given. The number of metaphase nuclei examined is followed by the chromosome number. If ploidy varied among nuclei from the same tumor, a range is given, followed by the modal chromosome number (in parentheses). Each chromosomal aberration detected is defined, together with the frequency with which it was observed among metaphase nuclei. t, translocation; (reciprocal), reciprocal translocation. Rb, Robertsonian; dic, dicentric; N.D., none detected. A translocation is defined as clonal if present in ≥ 75% of metaphase nuclei examined.

Mouse	Genotype	Lineage	Phenotype	Metaphases examined	Chromosome Number	Aberrations	Frequency
2207	WT/WT, *Trp53*$^{-/-}$	T cell	CD4^{+}CD8^{+}	10	43–45 (45)	Rb(5;5)	10/10
						Rb(6;6)	10/10
						Rb(16;16)	10/10
						Rb(17;15)	10/10
						Rb(1;1)	4/10
2319	WT/WT, *Trp53*$^{-/-}$	T cell	CD4^{+}CD8^{+}	10	67–69 (69)	dic(5;5)	10/10
3265	WT/WT, *Trp53*$^{-/-}$	T cell	CD4^{+}CD8^{+}	14	47	N.D.	14/14
3486	WT/WT, *Trp53*$^{-/-}$	T cell	CD4^{+}CD8^{+}	14	35–42 (41)	N.D.	14/14
2266	WT*/WT*, *Trp53*$^{-/-}$	T cell	CD4^{+}CD8^{+}	6	42	N.D.	6/6
2409	T490A/WT, *Trp53*$^{-/-}$	T cell	CD4^{+}CD8^{+}	9	29–38 (37)	t(17;14)	9/10
						t(4;16) (reciprocal)	9/10
						t(15;1)	1/10
						Rb(5;5)	10/10
						Rb(15;15)	10/10
						Rb(X;X)	9/10
2371	T490A/WT, *Trp53*$^{-/-}$	T cell	CD4^{+}CD8^{+}	7	37–47 (47)	t(7;14;15;5)	7/7
						t(7;5;15)	7/7
						t(16;14)	6/7
						t(7;16;15)	6/7
2361	T490A/WT, *Trp53*$^{-/-}$	T cell	CD4^{-}CD8 ISP	7	27–43 (43)	Rb(5;5)	3/7

Mouse	Genotype	Lineage	Phenotype	Metaphases examined	Chromosome Number	Aberrations	Frequency
						t(3;16)	1/7
2297	T490A/T490A, *Trp53*$^{-/-}$	T cell	CD4^{-}CD8 ISP	16*	37–46 (44)	t(2;5) (reciprocal)	6/6†
						t(12;14)	12/16††
2415	T490A/T490A, *Trp53*$^{-/-}$	T cell	CD4^{-}CD8 ISP	10	35–44 (42)	t(4;14)	10/10
						t(19;16)	9/10
						Rb(4;4)	9/10
						Rb(17;15)	9/10
2352	T490A/T490A, *Trp53*$^{-/-}$	T cell	CD4^{-}CD8^{-}	14	58–65 (60)	t(17;14;1)	13/14
						t(14;15)	1/14
						Rb(4;4)	14/14
2118	T490A/WT, *Trp53*$^{-/-}$	B cell	B220^{+}IgM^{+}IgD^{+}	10	28–40 (40)	t(10;12)	10/10
						t(10;19)	1/10
2135	T490A/WT, *Trp53*$^{-/-}$	B cell	B220^{+}IgM^{+}IgD^{+}	12	47	t(12;16)	12/12

*6 metaphases analyzed by SKY; 10 metaphases analyzed by painting chromosomes 12 and 14.

†Only metaphases analyzed by SKY included.

††Combined results of SKY and chromosome painting.